Spatially Variant Ultrasound Attenuation Mapping using a Regularized Linear Least-Squares Approach

Jasleen Birdi, *Member, IEEE,* Jan D'hooge and Alexander Bertrand, *Senior Members, IEEE*

Abstract—Quantitative ultrasound methods aim to estimate the acoustic properties of the underlying medium, such as the attenuation and backscatter coefficients, and have applications in various areas including tissue characterization. In practice, tissue heterogeneity makes the coefficient estimation challenging. In this work, we propose a computationally efficient algorithm to map spatial variations of the attenuation coefficient. Our proposed approach adopts a fast, linear least-squares strategy to fit the signal model to data from pulse-echo measurements. As opposed to existing approaches, we directly estimate the attenuation map, i.e., the local attenuation coefficient at each axial location by solving a joint estimation problem. In particular, we impose a physical model that couples all these local estimates and combine it with a smoothness regularization to obtain a smooth map. Compared to the conventional spectral log difference method and the more recent ALGEBRA approach, we demonstrate that the attenuation estimates obtained by our method are more accurate and better correlate with the ground-truth attenuation profiles over a wide range of spatial and contrast resolutions.

I. INTRODUCTION

THe technique of ultrasound imaging aims to provide a qualitative representation of the tissue of interest. This is complemented by the field of quantitative ultrasound (QUS) [1], [2], where the goal is to obtain a quantitative mapping of the underlying tissue by estimating its acoustic properties from the backscattered ultrasound signal. The QUS techniques have gained attention by showing the potential for cancer imaging [3], cancer therapy monitoring and assessment [4], and kidney function monitoring [5], among various other application areas. Of primary importance in QUS are the attenuation and backscatter coefficients. Various studies have shown these coefficients to be invaluable for tissue characterization and diagnostic studies, such as in liver [6]–[8], bone [9], thyroid [10], breast [11], uterine cervix [12], placenta [13] and muscle [14]. These promising results have not only increased interest in QUS, but have also focused attention towards improving the existing methodologies to get even more accurate results.

A challenge in attenuation coefficient estimation relates to the heterogeneity of the signal propagation path from the transducer to the depth of interest. An accurate mapping of such a spatially variant attenuation coefficient is of relevance

J. Birdi is with the Lab on Cardiovascular Imaging and Dynamics in the Department of Cardiovascular Sciences, and the STADIUS Center for Dynamical Systems, Signal Processing, and Data Analytics in the Department of Electrical Engineering (ESAT), KU Leuven, Belgium. e-mail: (jasleen.birdi@kuleuven.be).

J. D'hooge is with the Lab on Cardiovascular Imaging and Dynamics in the Department of Cardiovascular Sciences, KU Leuven, Belgium

A. Bertrand is with the STADIUS Center for Dynamical Systems, Signal Processing, and Data Analytics in the Department of Electrical Engineering (ESAT), KU Leuven, Belgium.

for quantitative examination of the medium, in order to show contrast between regions that otherwise would appear the same in a standard B-mode image.

In this context, the conventional techniques relying on spectral analysis of the backscattered radiofrequency (RF) signal include the spectral shift method [15], which measures the centre frequency downshift of the spectrum, and, the spectral difference and spectral log-difference (SLD) methods [7], [16], [17], which measure the amplitude decay in the backscattered signal. A hybrid method was also proposed in [18], which is based on a combination of the spectral shift and spectral difference methods. The accuracy of the estimates obtained by these techniques is reported to be improved by recent methods. One such approach, developed in [19], employed a linear least-squares formulation to simultaneously estimate the attenuation and backscatter coefficients. Rather than an independent treatment of the attenuation coefficients at each axial position, other techniques in the literature added mechanisms to impose spatial smoothness of the attenuation coefficients across neighboring axial locations. A core ingredient in these methods was to regularize the coefficients along the depth dimension. The conventional SLD method was improved upon by the authors in [20], using a isotropic total variation (TV) regularization for attenuation estimation, under the assumption of a piece-wise homogeneous medium and the resulting problem was solved using the alternating direction method of multipliers algorithm [21]. Similarly, a TV based strategy solved using iteratively reweighted least squares was adopted in [22], indicating the potential of their approach to deal with heterogeneous tissues. The work in [23] further proposed a spatially weighted TV regularization scheme to deal with tissue heterogeneity. Another method based on dynamic programming (DP) exploited piece-wise continuity of the target coefficients using an ℓ_2 [24] and ℓ_1 regularization [25] strategy. It was shown to provide more accurate estimates than [19].

The aforementioned methods come with several drawbacks which hamper their use in practice. One of the main issues is the high computational complexity, in particular for the DP-based methods. Furthermore, their accuracy is highly variable, and in the case of DP strongly depends on the availability of good priors, i.e., a-priori known intervals that contain the actual attenuation coefficient, in order to narrow down the search space. These problems have recently been alleviated by the use of much faster linear least-squares (LLS) estimators, which result in an analytical solution, allowing to compute the relevant coefficients in a single shot by means of a simple inner product between a pre-computed matrix and the data [26],

[27]. Such a fast approach was first proposed in [26] for the case of piece-wise homogeneous regions. A similar approach, which also allows fully heterogeneous media, was independently proposed in [28], where it was termed 'ALGEBRA'. Not only are these methods much faster, they also substantially outperform DP-based methods, as demonstrated in [27], [28]. The existence of an analytical closed-form solution also makes them amenable to a real-time implementation [29].

When dealing with a heterogeneous medium, the previously mentioned DP, ALGEBRA and TV based methods estimate the effective (i.e. accumulated) attenuation coefficient, from the transducer to each axial depth point separately, possibly in combination with a smoothness regularizer. In practice, the actual local attenuation coefficient might be more relevant, e.g., for generating attenuation maps to distinguish between different intervening tissues. In such scenarios, these techniques must extract the local coefficient from the corresponding estimated averaged coefficient, e.g., by taking weighted differences between the effective attenuation coefficients at neighbouring depth points, which might again result in noisy estimates. On the other hand, the performance of existing local attenuation estimators, such as SLD, is reported to be severely impacted by the chosen data block size for which a local attenuation coefficient is estimated as well as the heterogeneity of the medium within that block [30]. In practice, a large data block size is needed to obtain an acceptable estimation accuracy with sufficiently low variance. However, such large data block sizes severely impact the spatial resolution of the resulting attenuation map, while at the same time increasing the risk of having tissue heterogeneity within the block itself.

Keeping the above points in mind, in the current work, we propose a fast LLS-based estimator, which directly estimates the attenuation map, i.e., it explicitly estimates the local attenuation coefficients at each depth point in the axial direction, with a low variance and high accuracy. This strategy comes with two advantages. First, it avoids the aforementioned post-processing to transform the effective (average) attenuation coefficients into local attenuation coefficients, which generates additional estimation noise that is not explicitly taken into account in the optimization process of the estimator itself. Second, it allows to impose a physical model which describes the interaction between the local attenuation coefficients towards the attenuation profile of the ultrasound wave over the entire axial depth. Such a coupling through a physical model is not included in the previously discussed methods. The regularized approaches, such as ALGEBRA, only link the (effective) attenuation coefficient estimates at different depths through a generic (model-free) spatial smoothing mechanism based on an ℓ_2-norm regularization.

As a starting point, we use the fast LLS framework reported in [26], [27]. While [27] only covers the case of homogeneous tissue, [26] also considers piece-wise homogeneous media, but requires prior knowledge of the locations of the boundaries between the different homogeneous layers. Our method does not require such prior knowledge, nor does it explicitly impose the attenuation profile to be piece-wise homogeneous. Instead, we divide the propagation medium in thin slices and model the per-slice attenuation through a joint physical propagation model over the full axial direction. The latter intrinsically results in a model-based coupling between all the attenuation estimates at different depths. To further guide the estimates towards a smooth attenuation map, we also add a (weighted) ℓ_2-norm regularization. We provide a performance evaluation of our proposed method and compare it with two state-of-the-art benchmarks (SLD and ALGEBRA) on both simulated and tissue-mimicking phantom data. Furthermore, we study the trade-off between the estimation accuracy on the one hand, and the spatial (axial) resolution and contrast resolution on the other hand.

The rest of the manuscript is organized as follows. We describe the proposed signal model and the approach developed for the attenuation coefficient estimation in section II. The studies performed and the datasets used for the method's validation are detailed in section III. We then present the results obtained in section IV, followed by their discussion in section V. Section VI provides the concluding remarks.

II. ESTIMATION OF THE ATTENUATION MAP

A. Acoustic Signal Model

Consider an acoustic wave, transmitted by a transducer and propagating through a weakly scattering medium of interest. The magnitude spectrum at frequency f of the signal backscattered from a region at depth z can be modelled as [19], [17]:

$$|S(f,z)| = |P(f)|\, D(f,z)\, A(f,z)\, B(f,z), \qquad (1)$$

where $P(f)$ stands for the transducer related effects, including the electrical signal's spectrum used for the transducer excitation as well as other coupling effects. $P(f)$ can be experimentally obtained as $\tilde{P}(f)$ from a pulse-echo reflector measurement in water, up to an unknown scaling G accounting for the uncertainty in the actual energy transmitted to the medium. Therefore, we define $P(f) = G\tilde{P}(f)$.

The term $D(f,z)$ incorporates the diffraction effects. Considering plane wave propagation, these effects can be neglected, i.e., $D(f,z) \approx 1$. This assumption, however, does not limit the applicability of our method. In case of non-negligible diffraction effects, they can be compensated for by means of a reference phantom measurement, similar to [19], [27].

$A(f,z)$ in (1) denotes the cumulative attenuation of the sample. In the case of soft tissues, the typical power-law frequency dependence of the attenuation reduces to a linear frequency dependence [31], [32] and under this assumption, we have $A(f,z) = \exp(-2\alpha(z)fz)$, where $\alpha(z)$ is the effective (accumulated) attenuation coefficient over a distance z in the axial direction. The factor 2 represents a forward and backward path, as we assume a pulse-echo recording.

Finally, $B(f,z)$ in (1) is the backscatter coefficient (BSC) as a function of frequency and depth. Using a power law frequency dependence model, we get $B(f,z) = B_0'(z)\, f^{\mu(z)}$, where, for a depth z, $B_0'(z)$ and $\mu(z)$ represent the BSC at 1 MHz and the associated frequency dependence, respectively.

Combining all this together, the backscattered signal model can be expressed as

$$|S(f,z)| = G\, |\tilde{P}(f)|\, e^{-2\alpha(z)fz}\, B_0'(z) f^{\mu(z)}. \qquad (2)$$

In the current work, we consider a medium with spatially varying attenuation and/or backscatter characteristics. Such a spatially variant region can be modelled as a concatenation of thin slices forming a multi-layered region with each layer having a constant value of the target coefficient. By making the slices thin enough, we can model any profile up to a pre-selected spatial resolution. Let us assume the region of interest be divided in L slices, each with a thickness Z. Every l^{th} slice, with $l \in \{1, \dots, L\}$, is probed at a depth location z_l (we typically choose z_l to be the centre coordinate of the lth slice) and α_l is the associated local attenuation coefficient of the lth slice. Similarly, denoting the BSC terms at depth z_l by $(B_0')_l$ and μ_l, the backscattered signal from a depth z_l can be modelled as

$$|S(f, z_l)| = G\,|\tilde{P}(f)|\,e^{-2\alpha_1 f Z}\,e^{-2\alpha_2 f Z}\,\dots e^{-2\alpha_{l-1} f Z}$$
$$e^{-2\alpha_l f(z_l - (l-1)Z)}\,(B_0')_l f^{\mu_l}. \quad (3)$$

It is straightforward to see that our model draws a relationship between the backscattered signal at any depth z_l and the medium's local attenuation coefficients at all previous positions. This is clearly in contrast with other approaches in the literature that link the signal with an effective (accumulated) attenuation coefficient, in which all the exponentials in (3) collapse into a single exponential [24], [28].

B. Proposed approach

The signal model in (3) exhibits a non-linear relation between the measured signal and the coefficients to be estimated. For computational efficiency, we propose to apply a logarithmic transform on both sides of the equation to obtain a linear model [26], [27]. This results in

$$\log|S(f, z_l)| = \log|G\tilde{P}(f)(B_0')_l| - 2\alpha_1 f Z - 2\alpha_2 f Z - \dots$$
$$- 2\alpha_{l-1} f Z - 2\alpha_l f(z_l - (l-1)Z) + \mu_l \log f. \quad (4)$$

Defining $Q(f, z_l) = \log|S(f, z_l)| - \log|\tilde{P}(f)|$, the above equation becomes

$$Q(f, z_l) = \log|(B_0)_l| - 2\alpha_1 f Z - 2\alpha_2 f Z - \dots - 2\alpha_{l-1} f Z$$
$$- 2\alpha_l f(z_l - (l-1)Z) + \mu_l \log f, \quad (5)$$

where $(B_0)_l = G(B_0')_l$. $Q(f, z_l)$ on the left-hand side captures quantities that can be measured from actual recorded data, i.e., the spectrum of the backscattered pulses $S(f, z_l)$ as well as the spectrum $\tilde{P}(f)$, which was already assumed to be known from a pulse-echo reflector measurement. Our goal is then to find the unknown parameters in the right-hand side of (5), i.e., B_0, α and μ values, such that the equation is satisfied as well as possible. As we are only interested in the attenuation map, the values B_0 and μ are viewed as byproducts in order to make the model complete as well as to cope with spatially varying acoustical properties within the medium. Note that the variable B_0 is not purely related to backscatter as it also absorbs the gain calibration factor G, which is assumed unknown.

Let us stack the measurements $Q(f, z_l)$ for all the L slices into a column vector $\mathbf{q}(f)$ of size $L \times 1$. We thus obtain

$$\mathbf{q}(f) = [Q(f, z_1), Q(f, z_2), \dots Q(f, z_L)]^T, \quad (6)$$

where $(.)^T$ denotes transpose of its argument. The right-hand side terms of (5) can be rearranged in the same manner to get the matrix $\mathbf{A}(f)$ as given in (7), and $\theta = [\log|(B_0)_1|, \dots, \log|(B_0)_L|, \alpha_1, \dots, \alpha_L, \mu_1, \dots, \mu_L]^T$. Corresponding to (5), the matrix equation for all the L slices thus becomes $\mathbf{q}(f) = \mathbf{A}(f)\,\theta$. Further, the spectrum, computed over a predefined window length that is centred at each slice's depth location, is analysed for N frequency points within the relevant bandwidth. The equations associated with each of the frequency points can be stacked together to get the matrix equation for the whole measurement process:

$$\mathbf{q} = \mathbf{A}\,\theta, \quad (8)$$

where $\mathbf{q} = [\mathbf{q}(f_1) \dots \mathbf{q}(f_N)]^T$ and $\mathbf{A} = [\mathbf{A}(f_1) \dots \mathbf{A}(f_N)]^T$. This corresponds to a linear system of equations with the unknowns gathered in the vector θ. An estimate of the unknowns can be obtained by solving these equations in least squares sense [33], i.e., by minimizing the total squared error between both sides of the equation as will be explained further on.

It is important to note that our adopted formulation intrinsically couples the different α values through a joint physical model, i.e., for every $l \in \{1, \dots, L\}$, α_l appears in multiple equations. This is different from the existing approaches such as SLD and ALGEBRA, where the attenuation coefficient is estimated separately at each depth point. In this case, the physical model does not impose an interaction between the attenuation estimates at different depth points. Nevertheless, regularization based methods, such as ALGEBRA impose some interaction between the different attenuation estimates by applying a standard spatial smoothness regularization to enforce that the attenuation estimates at neighbouring depth points are similar. Such regularization procedures are standard practice in estimation theory in case an estimator exhibits a large variance. Although the α-interactions enforced by our physical model (5) result in a smaller bias on the estimator, we empirically observed that a regularization is still required to achieve an estimator with a sufficiently low variance.

The choice of the regularization term depends on the underlying attenuation profile. Similar to [20], [24], [28], we assume that the attenuation coefficients spatially exhibit smooth variation in their values and thus, a suitable Tikhonov regularization term enforcing this continuity could be exploited. In line with these works, similar regularization strategies were used for BSC (B_0 and μ) as well. For instance, for a gradually varying profile, ℓ_2 regularization applied on the differences between the target coefficient values at consecutive depths is a good choice in general. On the other hand, for a profile where the coefficient values are fairly constant but undergo a sudden change at an unknown position, a sparsity imposing regularization, such as ℓ_1 regularization, on the consecutive coefficient differences might be more suitable. However, these ℓ_1 based regularizations do not have a closed form solution and therefore, typically have a higher computational cost than estimators based on ℓ_2 regularization. It has been reported in the literature that iteratively re-weighted ℓ_2 regularization could be considered as a good approximation to the ℓ_1 based regularizations [34]. We thus only explore the ℓ_2 norm and

$$\mathbf{A}(f) = \begin{bmatrix} 1 & 0 & \ldots & 0 & -2fz_1 & 0 & \ldots & 0 & \log f & 0 & \ldots & 0 \\ 0 & 1 & \ldots & 0 & -2fZ & -2f(z_2 - Z) & \ldots & 0 & 0 & \log f & \ldots & 0 \\ \vdots & \vdots & \vdots & \vdots & \vdots & \vdots & \vdots & \vdots & \vdots & \vdots & \vdots \\ 0 & 0 & \ldots & 1 & -2fZ & -2fZ & \ldots & -2f(z_L - (L-1)Z) & 0 & 0 & \ldots & \log f \end{bmatrix}_{L \times 3L} \tag{7}$$

the re-weighted ℓ_2 norm regularization given its low computational cost.

In this respect, we propose to obtain estimates of the target coefficients by solving the following linear least-squares minimization problem with Tikhonov regularization:

$$\underset{\theta}{\text{minimize}} \; \|\mathbf{q} - \mathbf{A}\theta\|_2^2 + \sum_{i=1}^{3} \lambda_i \|\mathbf{W}_i \Gamma_i \theta\|_2^2, \tag{9}$$

where the first term is the data-fidelity term and the second term is the ℓ_2 based regularization term for each of the parameters of interest as indexed by i ($i = 1, 2$ and 3 for B_0, α and μ, respectively), associated with the regularization parameter $\lambda_i > 0$. For every $i \in \{1,2,3\}$, $\mathbf{W}_i$ represents the weight matrix in the re-weighted ℓ_2-norm approach, which will be defined later on. The matrix Γ_1 is designed to compute the differences between the neighbouring backscatter coefficients B_0 in θ. Mathematically, $\Gamma_1 = [\Delta \quad \mathbf{0} \quad \mathbf{0}]$, where Δ is the difference-computing matrix given by

$$\Delta = \begin{bmatrix} 1 & -1 & 0 & \ldots & 0 & 0 \\ 0 & 1 & -1 & \ldots & 0 & 0 \\ \vdots & \vdots & \vdots & \vdots & \vdots \\ 0 & 0 & 0 & \ldots & 1 & -1 \end{bmatrix}_{(L-1) \times L}, \tag{10}$$

$\mathbf{0}$ is the zero matrix of size $L - 1 \times L$. Similarly, these differences for the neighbouring α and μ values are computed by $\Gamma_2 (= [\mathbf{0} \quad \Delta \quad \mathbf{0}])$ and $\Gamma_3 (= [\mathbf{0} \quad \mathbf{0} \quad \Delta])$, respectively.

Equation (9) has a closed form solution given by [33]

$$\hat{\theta} = (\mathbf{A}^T \mathbf{A} + \sum_{i=1}^{3} \lambda_i (\mathbf{W}_i \Gamma_i)^T (\mathbf{W}_i \Gamma_i))^{-1} \mathbf{A}^T \mathbf{q}. \tag{11}$$

Concerning the weight matrix, when considering simple ℓ_2 regularization, the weights are set to unity, i.e., for $i \in \{1,2,3\}$, $\mathbf{W}_i = \mathbf{I}$ and the resulting problem has the aforementioned closed-form solution. We refer to this approach as LLS-l2. If weighted ℓ_2 regularization needs to be applied, the estimates $\hat{\theta}$ are first obtained by the LLS-l2 approach. Using these estimates, each $\mathbf{W}_i$ is built as a diagonal matrix where the j-th diagonal entry is defined as $(w_i)_{jj} = 1/((\Gamma_i \hat{\theta})_j + \epsilon)$, where $(\Gamma_i \hat{\theta})_j$ is the j-th entry in the vector $(\Gamma_i \hat{\theta})$, and $\epsilon > 0$ is typically a small value, used for stability purposes [35], [36]. The problem is then again solved using the closed form solution in (11) using the new weighting matrix. We only apply one such re-weighting iteration for computational efficiency, and because additional iterations were empirically found to not improve the result. We refer to this approach as LLS-wl2.

It is worth highlighting here that our proposed approach, whether LLS-l2 or LLS-wl2, can also be applied when the reference phantom measurements are available to correct for system-dependent diffraction effects [17]. It basically involves

taking the ratio of the magnitude spectrum of the signal backscattered from the same depth of the target and reference medium, using the signal model (3). The logarithmic transform and the matrix formulation is then computed using this ratio and the rest of the approach follows. The coefficient values for the reference medium are known, and hence, those of the target medium can be extracted from the solutions obtained using the adopted approach. For the interested reader, we refer to [27], [28] for a more detailed explanation.

C. Computational complexity

The closed form solution in (11) can be rewritten as $\hat{\theta} = \mathbf{V}\mathbf{q}$, where $\mathbf{V} = (\mathbf{A}^T \mathbf{A} + \sum_{i=1}^{3} \lambda_i (\mathbf{W}_i \Gamma_i)^T (\mathbf{W}_i \Gamma_i))^{-1} \mathbf{A}^T$ is data independent. For LLS-l2, with weights $\mathbf{W}_i$ set to unity, the matrix $\mathbf{V}$ can be computed a-priori. As a result, the estimator (11) boils down to a single matrix-vector multiplication, thereby facilitating an efficient real-time computation [29]. In the case of LLS-wl2, the weights $\mathbf{W}_i$ become data-dependent, in which case the matrix $\mathbf{V}$ needs to be computed at run-time. The pre-computed matrices $\mathbf{A}$ (and thus, $\mathbf{A}^T \mathbf{A}$ and $\mathbf{A}^T$) and Γ_is can, however, still be used.

The computation of the data vector $\mathbf{q}$ requires the computation of the RF spectra at different axial depths, which scales linearly with the number of slices L. This computation can make use of efficient algorithmic routines based on the fast Fourier transform (FFT) [37].

III. MATERIALS & METHOD

A. Data generation

The performance of the proposed method was assessed on both simulated and tissue-mimicking phantom data, the details of which are provided below.

1) Synthetic data: We considered several 90 mm thick mediums with spatially varying α values. The backscattered signal from a one-dimensional uniform distribution of point scatterers, placed in a flat, unfocused single element transducer's far field, was modelled based on (3), which was then coherently summed up across all point scatterers in the time domain to generate the RF lines [27]. A total of 500 RF lines were generated by considering different realization of the random scatterers positions in the medium. Using these lines, 10 datasets were obtained, where each dataset included 50 randomly picked RF lines from the total lines. The speed of sound in the propagation medium was considered to be 1500 m/s. The transmitted pulse had a Gaussian spectrum, with 1.36 mm pulse length, centre frequency of 3 MHz and fractional bandwidth of 80%.

Focusing on mapping the spatial variations of the attenuation coefficient, the first tests considered a fixed value of the backscatter coefficient, i.e., for every $l \in \{1, \ldots, L\}$,

TABLE I

Acoustic properties of the sample phantoms used in the reference phantom measurement experiments. α is in units of dB/cm/MHz, $\bar{B}_0$ in $(cm\text{-}sr\text{-}MHz^{\bar{\mu}})^{-1}$ and $\bar{B} = \bar{B}_0 f^{\bar{\mu}}$ in $(cm\text{-}sr)^{-1}$. The BSC values are given with respect to the backscattered signal's power spectrum model.

Phantom	Layer	α	$\bar{B}_0 (= B'^2_0)$	$\bar{\mu}$	$\bar{B}$ (at 8.9MHz)
A (uniform BSC)	1st & 3rd	0.510	1.60e-06	3.52	3.52e-03
	2nd	0.779	3.22e-06	3.13	3.02e-03
B (uniform attenuation)	1st & 3rd	0.554	4.82e-07	3.80	3.52e-03
	2nd	0.58	3.94e-06	3.38	6.37e-03

$(B'_0)_l = 10^{-4}(\text{cm-sr})^{-1}$ and $\mu_l = 0.5$. For the spatially varying α values, we studied two attenuation profiles. The first one resembles a step-function profile, characterized by sharp changes in the attenuation values and illustrated in fig. 1 (left) as a blue line, referred to as the step profile hereafter. Such a profile can be observed in clinical applications, for instance, when the wave traverses a soft-tissue, followed by bone [38]. The second attenuation profile is simulated as a trapezoidal-shaped function as indicated by the blue line in fig. 1 (right). In this case, the α values change more smoothly, e.g., as in the boundary between fat and muscle layers [39].

We further investigated the axial spatial and contrast resolution achievable by our method. For spatial resolution evaluation, the mid-layer thickness of both profiles was varied from 30 to 5 mm while keeping the α values of the layers fixed. For the step profile, this corresponded to $\alpha = 0.7$ dB/cm/MHz for the two outermost/background layers and $\alpha = 1$ dB/cm/MHz for the mid-layer. For the trapezoidal profile, the layers over the first 30 mm had an α value linearly increased from 0.6 to 1 dB/cm/MHz, followed by a mid-layer with constant α = 1 dB/cm/MHz and then a gradual descent such that it hits 0.6 dB/cm/MHz at both edges of the profile. The two regions with $\alpha = 0.6$ dB/cm at the two edges will be referred to as the background/outermost layers. For contrast evaluation, the α contrast was defined as the ratio of the difference between the α values of the mid-layer and the background, and the α value of the background. The mid-layer α value was varied to have contrast values ranging from 100 to 5%, while keeping the thickness of the mid-layer fixed to 30 mm.

Finally, to examine the accuracy of the estimated attenuation map in a medium with varying BSC, we generated a dataset with backscattered signals from a three-layered medium, each layer being 30mm thick, where the backscatter term behaves as a step function in the axial direction. The mid-layer had a 10 dB higher BSC ($B_0 = 9 \times 10^{-4}(\text{cm-sr})^{-1}$, $\mu = 1.2$) than the other two layers ($B_0 = 2 \times 10^{-4}(\text{cm-sr})^{-1}$, $\mu = 1.5$), whereas the attenuation coefficient was nearly the same for the three layers (α (in dB/cm/MHz) = 0.7, 0.75 and 0.7, respectively for the three layers).

2) In-vitro data: Data acquired from two tissue-mimicking phantoms were used for further evaluation, as used previously and described in detail in [19], [28], [40]. Both phantoms were three-layered phantoms, composed of a mixture of ultrafiltered milk and water-based gelatin, exhibiting scattering properties due to the presence of solid glass-beads of 5-43 μm diameter thickness. The first phantom had a uniform backscatter, but

with a substantially higher attenuation in the second layer by varying the milk's amount in the mixture. On the contrary, the second phantom represents the case of uniform attenuation, but with a higher backscatter in the second layer as achieved by varying the glass-beads concentration.

For both phantoms, 10 uncorrelated RF data frames were acquired using a linear array 18L6 transducer, Siemens Acuson S2000 scanner and a center frequency of 8.9 MHz. The spectrum $\tilde{P}(f)$ was not known and reference phantom measurements were made using the same settings from the phantoms' top layers. The phantoms' ground truth α and BSC values were obtained using single-element transducers for the narrowband substitution and broadband pulse-echo techniques, respectively and are listed in Table I.

B. RF data processing

For the proposed method's implementation and performance evaluation, MATLAB was used. The given time-domain RF signal was divided into several overlapping windows, with adjacent windows having their centres separated by 25% of the window length ($\sim$ 3 mm, i.e., two pulse lengths) for the simulated data and 15% of the window length (4 mm) for the phantom data. The magnitude spectrum of the RF data in each window, corrected for spectral leakage using a Hanning window, was computed and then averaged over the considered RF lines. Moreover, the computed magnitude spectrum was considered only over a range of frequencies in order to remove the frequency regions that mostly consist of noise. This threshold determining the usable bandwidth was set to be 10 dB below the peak of the spectrum for both synthetic and phantom data. The choice of these parameters (window length, window overlap and usable bandwidth) was based on the results from [27], where an extensive parameter sensitivity study was performed to analyse the effect of these parameters on the estimates' accuracy.

Note that each center point of a window conceptually corresponds to a center point of a slice as defined in (3). Overlap between the windows then implies that a spectrum is computed over multiple slices. While this overlap improves the frequency resolution (i.e. the number of frequency points N), it will reduce the axial resolution of the attenuation map. However, this is acceptable because of the intrinsic smoothness assumption. Furthermore, the weighting with the Hanning window emphasizes the data points that are closest to the center of the current slice, such that the effect of overlap is reduced.

C. Benchmark methods

We used two methods for comparison: the standard SLD approach for local attenuation estimation and the more recently proposed ALGEBRA method.

The SLD approach relies on computing the log difference of the power spectrum obtained from the proximal and distal windows of the chosen data block size within the field of view (also sometimes referred to as the region of interest). Under certain assumptions on the BSC, the α value of the data block is obtained by fitting a straight line to the computed spectral log difference plotted as a function of frequency. The data block size needs to be tuned and has to be large enough to

obtain a reliable estimate. In our experiments, we found that a data block of 15 pulse lengths in the axial direction with 85% overlap gave reasonable results. For the phantom data, in the absence of exact pulse length knowledge, the data block length was selected to be 60 times the wavelength. The considered values were empirically found to provide a reasonable tradeoff between the spatial resolution and variance of the obtained solution and is in line with other works in the literature [20], [30].

Since ALGEBRA is designed to estimate the total or averaged attenuation up to a location z_l (instead of the local attenuation at z_l), the obtained averaged estimates $\alpha_{\text{avg}}(l)$ were transformed to the local attenuation domain as [28]

$$\alpha_{\text{local}}(l) = \frac{\alpha_{\text{avg}}(l)z_l - \alpha_{\text{avg}}(l-1)z_{l-1}}{z_l - z_{l-1}}, \qquad (12)$$

which were used for comparison with our proposed approach's estimates. It can be seen that retrieval of a local attenuation coefficient at a given depth relies on the estimated total attenuation at neighbouring depth points. This requires a subtraction of two estimated quantities, which leads to an increase in the estimation noise. ALGEBRA was applied on the considered data sets based on its proposed implementation in [28]. The algorithmic parameters, window length, window overlap and usable bandwidth, were set to be the same as for our proposed method to obtain a fair comparison. The regularization parameter was set differently for each method, as all methods require a different amount of smoothing. For ALGEBRA, the regularization parameters were set the same as in [28] when applied on the phantom data (as we employ the same data set here). For the simulated data, the regularization parameters were optimized for each method separately based on a parameter sweep in order to maximize performance.

D. Quantitative metrics for evaluation

The relative error of the estimated α in the mid-layer (α rel-err) was used as an accuracy metric. To quantify the overall reconstruction performance of the entire attenuation profile, we used the Normalized cross-correlation (Ncc) between the true (α_{true}) and estimated ($\hat{\alpha}$) attenuation profiles defined as

$$\text{Ncc} = \frac{\sum_{l=1}^{L}(\hat{\alpha}_l - \text{mean}(\hat{\alpha}))\left((\alpha_{true})_l - \text{mean}(\alpha_{true})\right)}{L(\sqrt{\text{var}(\hat{\alpha})\,\text{var}(\alpha_{true}))}}.$$
$$(13)$$

The higher the value of Ncc, the higher is the correlation between the estimated and the ground truth profile. Furthermore, since the full width at half maximum (FWHM) is a characteristic of the underlying profile, indicating its sharpness/degree of smoothness, we used the relative error of FWHM of the estimated α profile (FWHM rel-err) as a third metric. Note that for α rel-err and FWHM rel-err, lower is better, while for Ncc higher is better.

While examining the contrast resolution, an additional metric in the form of the relative error of the estimated α contrast was considered. For this purpose, median values of the estimates obtained in the mid-layer and the two outermost layers were used for contrast calculation.

IV. RESULTS

A. Comparison of different methods

1) Synthetic data results: Fig. 1 depicts the α profiles estimated by the considered methods when applied on the step and trapezoidal profiles. The ground truth profile in both cases is also shown. It can be seen that our proposed methods (LLS-l2, LLL-wl2) outperformed SLD and ALGEBRA, having a mean α rel-err < 10% and mean Ncc of $\sim$ 90% vs. respectively 17% and 60% for SLD, and 15% and < 75% for ALGEBRA. The FWHM rel-err was also lower for LLS-(w)l2 (< 10%) than that of SLD and ALGEBRA.

The relative error for μ estimation was around 10% for the proposed methods and ALGEBRA. Since this study focuses on the attenuation map estimation, we report only the results of the α estimation hereafter.

2) Phantom data results: The α profile estimation results on Phantom A with attenuation step are presented in Fig. 2, showing superior performance of our methods over the benchmark methods. This was in line with the quantitative assessment, with mean α rel-err (computed over the whole depth) of 15% (LLS-l2), 16% (LLS-wl2) compared to 43% for SLD and 19% for ALGEBRA. Along the same lines, the corresponding mean values for Ncc were 74% and 77% for LLS-l2 and LLS-wl2, respectively vs. 40% for SLD, 57% for ALGEBRA. Similarly, the observed mean values for the FWHM rel-err were the least for LLS-wl2 (14%).

B. Study on spatial and contrast resolution

a) Spatial resolution: The results obtained by varying the mid-layer thickness to probe the α profiles' spatial resolution are shown in figs. 3-4 for the estimated profiles representation and the quantitative assessment, respectively, for the step profile. It can be observed that as the mid-layer became narrower, the estimation performance degraded for all the methods. Overall, our methods (both LLS-l2 and LLS-wl2) exhibited superior performance, obtaining lower errors. The results suggest that they are able to estimate the layer down to 10 mm reasonably well, keeping mean α rel-err $\leq$ 10% till 10 mm, beyond which it increased. Ncc also decreased rapidly, from $\sim$85% at 10 mm mid-layer thickness to 20% for 2 mm mid-layer thickness. FWHM-rel err results supported these findings with a sharp increase in the error below 10 mm. SLD and ALGEBRA showed, for instance, only a small value of Ncc (40%) at 10 mm, with high FWHM-rel err.

Similar observations can be made for the trapezoidal profile results in figs. 5- 6. While performing better than the benchmark methods, having almost $10-15\%$ lower α rel-err and 40% higher Ncc, the proposed methods were able to estimate profiles even with 5 mm thick mid-layer.

b) Contrast resolution: Figs. 7 and 8 show the results when the α value of the step profile's mid-layer is varied. The qualitative representation of the estimated profiles indicates good performance of the methods in recovering the profiles for all contrast values. The quantitative plots in fig. 8, however, highlight a deterioration in the estimation quality for α contrast below 20%, except for the α rel-err, which exhibited a decreasing trend as the α contrast decreased. Overall, our methods
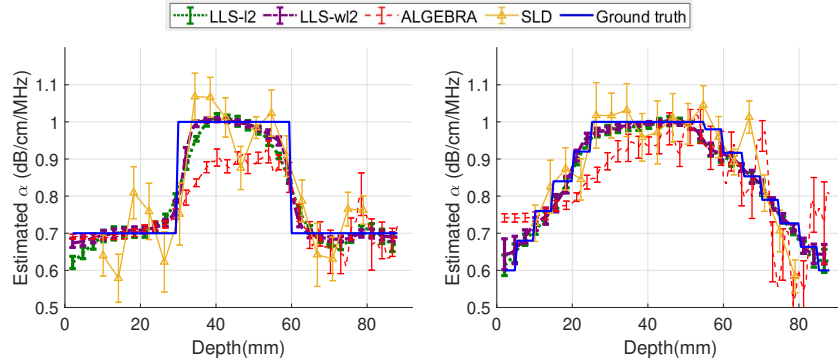
Fig. 1. Results of attenuation coefficient (α) profile estimation obtained by various methods on the simulated data with step profile (left) and trapezoidal profile (right). In each case, the mean estimated values are plotted, with the error bars denoting the standard deviation of the estimated values for 10 repetitions of the experiment.
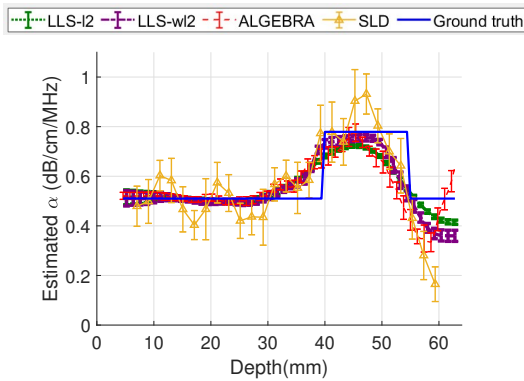

Fig. 2. Results of attenuation coefficient (α) profile estimation obtained by various methods on Phantom A with varying attenuation. In each case, the mean estimated values are plotted, with the error bars denoting the standard deviation of the estimated values for 10 RF data frames.

outperformed SLD and ALGEBRA, both qualitatively and quantitatively. For instance, unlike SLD and ALGEBRA, the mean α rel-err was below 10% for both LLS-l2 and LLS-wl2 for all contrast values. Similarly, our methods had lower FWHM-rel err and α contrast relative errors, which were $<$ 20% from 100% till 20% contrast value.

The results in figs. 9 and 10 for the trapezoidal profile also show better performance of our methods in estimating the α profiles than SLD and ALGEBRA. Moreover, the various metrics exhibited an almost flat trend when the contrast was decreased from 100% to 20%, compared to 50% reduction in mean Ncc for SLD and ALGEBRA. For contrast values $<$ 20%, Ncc and FWHM-rel err in particular deteriorated by $\sim$ 30% and $\sim$20%, respectively for the proposed methods.

C. Performance evaluation for spatially varying BSCs

Fig. 11 shows the results obtained for the case with varying BSC (and nearly uniform attenuation coefficient) for the phantom and simulated data in the left and right columns, respectively. While the α profiles estimated by LLS-l2, LLS-wl2 and ALGEBRA are close to the true ones, the estimated profile of SLD shows large deviations specifically at the points where the BSC changes. Quantitatively, for the simulated data, LLS-l2 and LLS-wl2 had relative α estimation errors (computed over the whole depth) of 3% and 7%, respectively,

vs. 39% for SLD and 20% for ALGEBRA. Similarly, for the phantom data, LLS-l2 and LLS-wl2 had relative α estimation errors (computed over the whole depth) of 6% and 5%, respectively, vs. 50% for SLD and 23% for ALGEBRA.

We also illustrate the estimated BSC profile for the LLS-l2 approach (the other methods' estimations are not shown for the sake of clarity of the figure) as a function of both frequency and depth. The estimated BSC profile can be seen to capture the spatial variations in BSC as present in the underlying ground-truth BSC profile.

V. DISCUSSION

We presented a regularized LLS approach to map the local attenuation variations in a heterogeneous medium of interest. Our method is based on a physical model that intrinsically incorporates the local attenuation coefficients and thus provides an implicit coupling between the different α estimates. Employing the LLS method to solve the underlying problem further provided a fast implementation of the estimator. We have thus proposed a methodology for accurate and fast estimation of the local attenuation coefficients.

The performance of the proposed approach was evaluated against the traditional spectral log difference (SLD) method and the more recently proposed ALGEBRA technique. The results demonstrated that our method outperformed the benchmark methods, providing local attenuation estimates with higher accuracy and lower variance. Here, it is noted that the total attenuation coefficients estimated by ALGEBRA were converted to local attenuation values at each depth position using a post-processing step, which makes it intrinsically prone to additional estimation noise. A notable difference between our method and the benchmark methods is that the latter rely on an isolated physical model for each depth point separately. For ALGEBRA, the different estimates are only coupled through a generic spatial smoothing regularization scheme. Our method, on the other hand, couples the estimated coefficients via both a smoothness regularization and the employed physical model itself, resulting in a superior performance. Our proposed approach was also tested on phantom data, estimating profiles in good agreement with the true profile.

A particular point of concern for the SLD method is the requirement of a sufficiently large data block size (of the
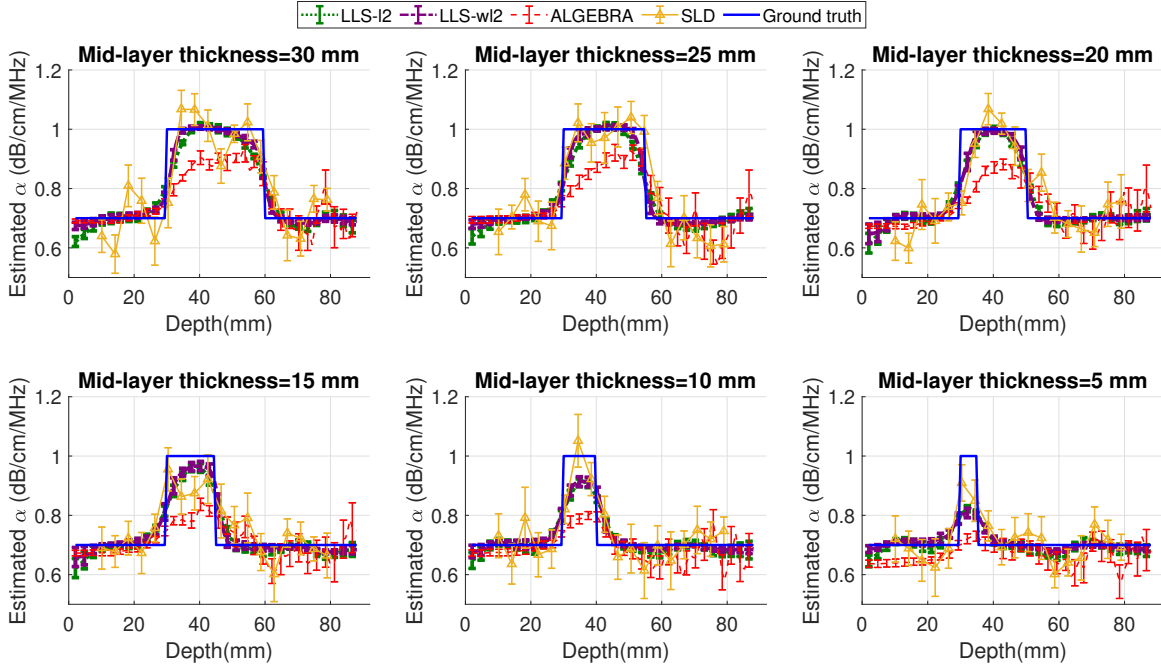
Fig. 3. Results of attenuation coefficient (α) profile estimation by various methods on the simulated data with step profile, varying the mid-layer thickness from 30 to 5 mm. In each case, the mean estimated values are plotted and the error bars denote the standard deviation of the estimated values for 10 repetitions of the experiment.
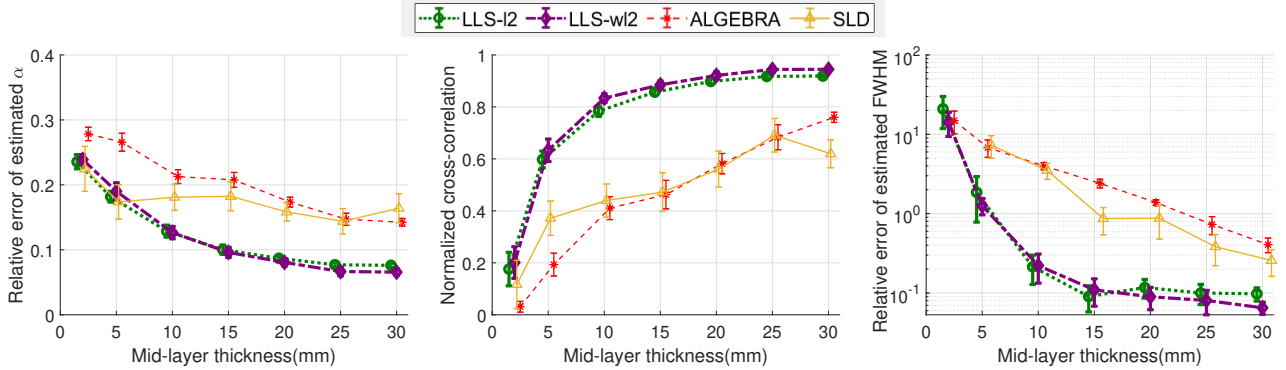

Fig. 4. Evaluation metric results for α profile estimation on the simulated data by various methods, as a function of mid-layer thickness of the step profile. From left to right, the relative error of the estimated mid-layer α, normalized cross-correlation between the true and estimated α profiles, and the relative error of the estimated FWHM are plotted. In each case, the respective mean metric values are plotted, with the error bars denoting the standard deviation of the values when the experiment is repeated 10 times.

order of tens of pulse lengths) to achieve reasonable estimation results. On the contrary, our approach is able to obtain good estimates with much smaller data block size, set equal to the window length and can be as small as twice the pulse length.

We further investigated the spatial and contrast resolution that can be achieved by these approaches on two types of α profiles - step and trapezoidal profiles characterizing sudden and gradual change in α values, respectively. In all cases, our approach outperformed the benchmark methods. For the spatial resolution study, it was observed that LLS-(w)l2 is able to estimate the layers well down to a thickness of 10 mm for the step profile, whereas it performed fairly well for all considered mid-layer thicknesses of the trapezoidal profile. This is expected as this smoothly varying profile is much easier to estimate than detecting sudden jumps in α values for the step

profile. Moreover, ℓ_2 based regularizations are generally well-suited to promote smoothness of its argument. Nevertheless, abrupt changes in the α value were still detectable in very thin step profiles with a thickness < 10 mm, although α is strongly underestimated in this case.

Concerning the contrast resolution, the proposed LLS-(w)l2 method was seen to perform well in recovering α profiles ranging from high (100%) to low (5%) contrast, with the mid-layer thickness of 30 mm. The quantitative metrics also maintained a high accuracy level until 20% α contrast, below which the errors started to increase for the step profile. This could, however, be due to the definition of the metrics. For instance, FWHM is in practice well-defined for the distributions with large peaks. This is not actually true for low contrast, where slight differences in the profile can significantly impact the
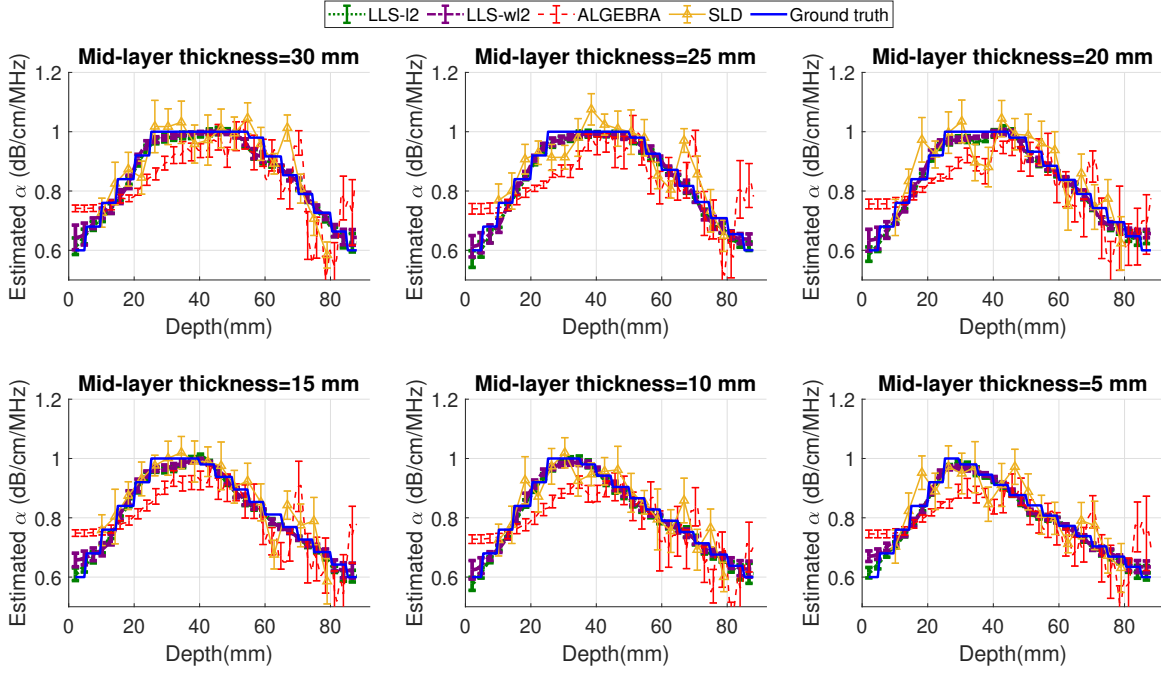
Fig. 5. Results of attenuation coefficient (α) profile estimation by various methods on the simulated data with trapezoidal profile, varying the mid-layer thickness from 30 to 5 mm. In each case, the mean estimated values are plotted and the error bars denote the standard deviation of the estimated values for 10 repetitions of the experiment.
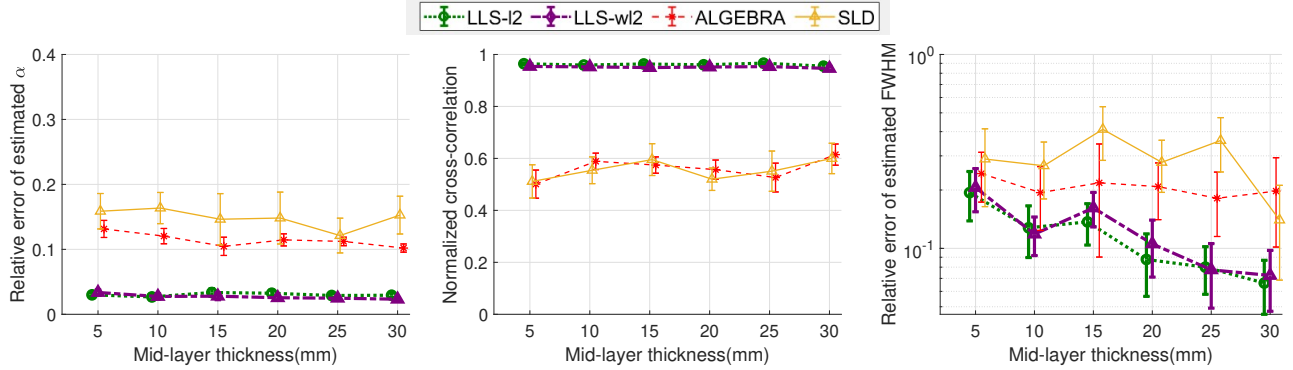

Fig. 6. Evaluation metric results for α profile estimation on the simulated data by various methods, as a function of mid-layer thickness of the trapezoidal profile. From left to right, the relative error of the estimated mid-layer α, normalized cross-correlation between the true and estimated α profiles, and the relative error of the estimated FWHM are plotted. In each case, the respective mean metric values are plotted, with the error bars denoting the standard deviation of the values when the experiment is repeated 10 times.

computed FWHM. An interesting observation pertained to the decreasing α rel-err over the entire contrast range for the step profile. With reduced contrast and thus, reduced height of the edges between the layers, the estimation within the whole mid-layer, specifically at the near-edge regions, matches the true values well, which could explain the decrease in α rel-err.

The focus of the current work was to provide an accurate α mapping for a medium with spatially varying acoustic properties. We thus also examined the attenuation estimation performance of our method and the benchmark methods in the case when the underlying medium exhibited spatial variations in the BSC. It was observed that while SLD estimations suffered specifically in the regions where the BSC changed, i.e. where the method's underlying assumption of uniform BSC within a single data block was violated, our method and

ALGEBRA performed fairly well in estimating the α profile. We further illustrated that the model in our proposed method is able to model the changes in the BSC without wrongfully attributing these discontinuities to changes in attenuation.

While LLS-l2 and LLS-wl2 were observed to have similar performances, slight differences can be noticed. The profiles estimated by LLS-wl2 were closer to the true profile, especially in the mid-layer and near the initial depth region, where estimates by LLS-l2 were slightly pulled down. Quantitatively also, LLS-wl2 scored metric values $\sim$ 1-5% better than that of LLS-l2. These observations were made for the step profile in each of the considered case studies. This is expected since the purpose of weighted ℓ_2 regularization is to approximate the sparsity promoting ℓ_1 regularization, which is more representative for a profile like the step profile
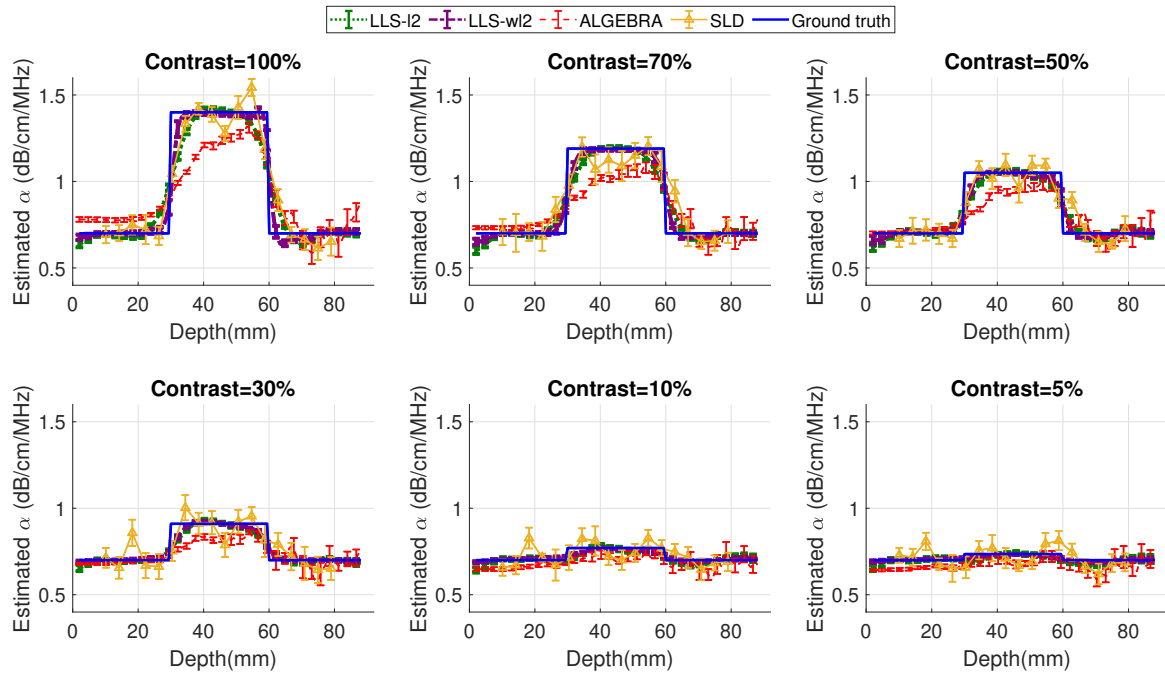
Fig. 7. Results of attenuation coefficient (α) profile estimation by various methods on the simulated data with step profile, varying the α contrast from 100 to 5%. In each case, the mean estimated values are plotted and the error bars denote the standard deviation of the estimated values for 10 repetitions of the experiment.
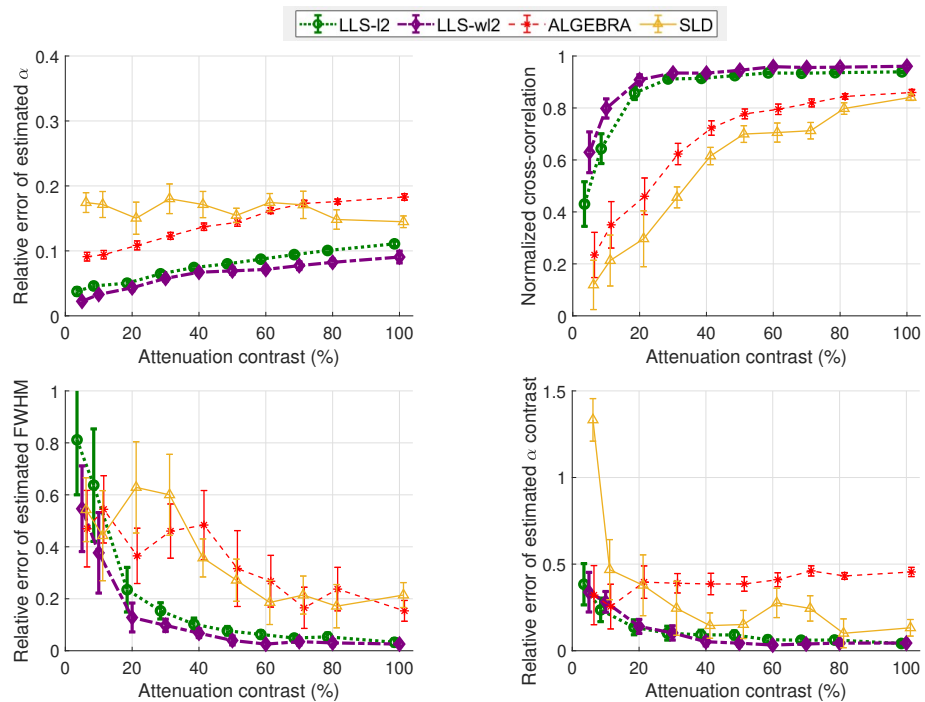

Fig. 8. Evaluation metric results for α profile estimation on the simulated data by various methods, as a function of α contrast of the step profile. The following are plotted: (top left) the relative error of the estimated mid-layer α, (top right) normalized cross-correlation between the true and estimated α profile; (bottom left) the relative error of the estimated FWHM and (bottom right) the relative error of the estimated α contrast. In each case, the respective mean metric values are plotted, with the error bars denoting the standard deviation of the values when the experiment is repeated 10 times.
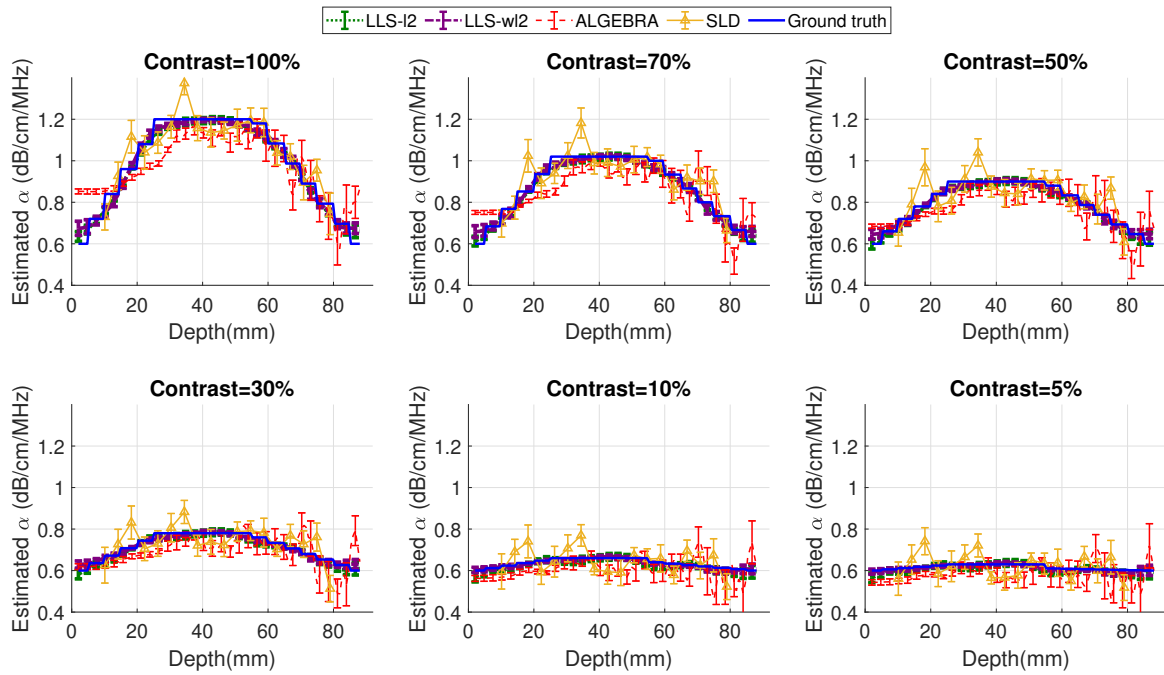
Fig. 9. Results of attenuation coefficient (α) profile estimation by various methods on the simulated data with trapezoidal profile, varying the α contrast from 100 to 5%. In each case, the mean estimated values are plotted and the error bars denote the standard deviation of the estimated values for 10 repetitions of the experiment.
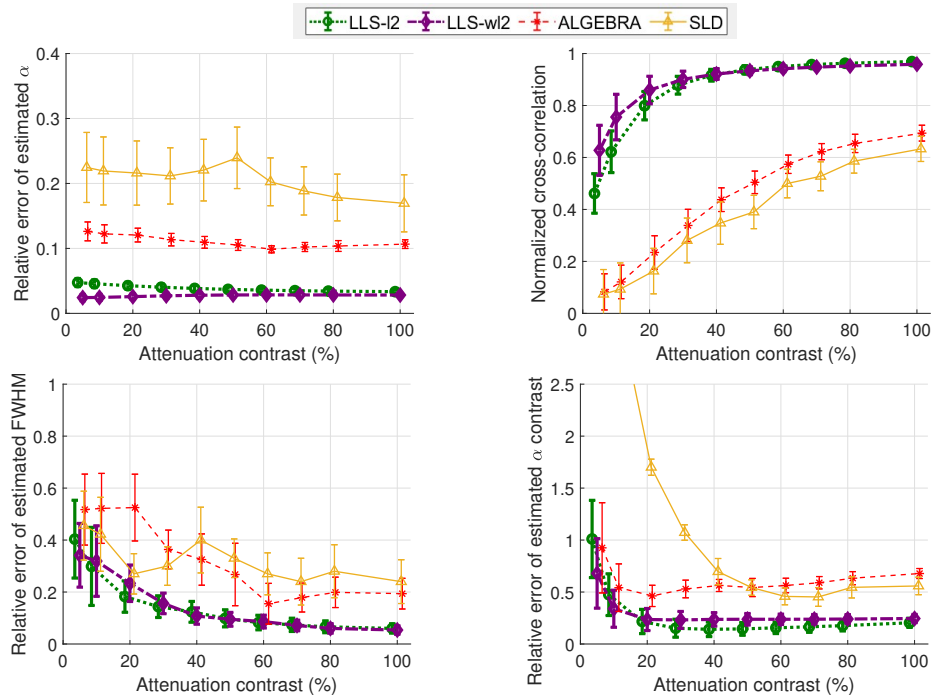

Fig. 10. Evaluation metric results for α profile estimation on the simulated data by various methods, as a function of α contrast of the trapezoidal profile. The following are plotted: (top left) the relative error of the estimated mid-layer α, (top right) normalized cross-correlation between the true and estimated α profile; (bottom left) the relative error of the estimated FWHM and (bottom right) the relative error of the estimated α contrast. In each case, the respective mean metric values are plotted, with the error bars denoting the standard deviation of the values when the experiment is repeated 10 times.

due to the sparse nature of the changes in α. Although with more weighting iterations, the approximation of the ℓ_1 norm would become better, preliminary results indicated no further improvement in the estimation accuracy and hence, we used only one weighted iteration. Note that performing the weighting iteration increases the computational cost as now, two iterations (one with LLS-l2, another with the computed weights for LLS-wl2) need to be performed.

In subsection II-C, we argued that the final solution (11) can be computed very efficiently in a real-time setting as all matrices involved (except the data vector $\mathbf{q}$) are independent of the data and thus, most of the matrix manipulations can be done a-priori. The computation of $\mathbf{q}$ is dependent on the number of slices, L, requiring L fast Fourier transforms (FFTs) to compute the spectra at each depth point. For instance, for the simulated datasets with 90 mm thick medium, $L = 128$, and in each of these cases, our MATLAB code provided the final solution using equation (11) in the order of seconds ($\sim$ 2-3 seconds). Smaller L values can further reduce the computational time, but at the cost of spatial resolution. Our first test with a real-time implementation of our previous LLS approach [27], i.e., for a homogeneous medium, has also shown promising results in experimental settings [29]. To enable translation of the proposed approach in clinical settings, even faster implementations can still be achieved by using C as the programming language, which is beyond the scope of the current study.

We further note that the extension of the proposed approach to generate 2D parametric α maps can be performed, similar to the 2D approach in [28], in which case a lateral spatial smoothing can be added. Finally, the promising results obtained by our proposed method motivates its more extensive testing in-vitro as well as in-vivo. This is, however, expected to come with its own set of challenges primarily due to a potential mismatch between the adopted model and the actual physical signal behaviour in real tissue. For instance, the current model assumes a linear frequency dependence of the attenuation coefficient, instead of a more general power law model. To mimic the latter, a possibility could be to apply the proposed approach over narrow frequency bands, where the linear approximation of the attenuation coefficient's frequency dependence could still be valid, and then combining these estimates [41]. Concerning BSC, currently a power law model is considered. For in-vivo application, the proposed approach will need to be adapted to a more generalized representation of BSC in terms of the form factor, which can be done along similar lines as reported in [42].

VI. Conclusion

A fast, regularized linear least-squares method was proposed for spatially varying local attenuation coefficient estimation. Our method differs from previous approaches in the literature as it couples the coefficients at all depth points via the adopted physical model. We further proposed two regularization schemes - ℓ_2 and weighted ℓ_2 regularization, with corresponding approaches being referred to as LLS-l2 and LLS-wl2, respectively. Their performances were tested on synthetic data, including both sharply and gradually changing α profiles, as well as on phantom data. Further, both synthetic and phantom data were considered for testing their performance when a spatially varying backscatter coefficient was introduced. Overall, while LLS-wl2 provided only slightly better estimates than LLS-l2 (specifically for the sharply varying α profile), both LLS-l2 and LLS-wl2 were shown to outperform the traditional spectral log difference method and the recent ALGEBRA method in terms of both accuracy and variance of the obtained estimates. The proposed methods also achieved a robust performance while recovering attenuation profiles with varying spatial as well as attenuation contrast resolution in the axial direction.

References

[1] F. L. Lizzi, M. Greenebaum, E. J. Feleppa, M. Elbaum, and D. J. Coleman, "Theoretical framework for spectrum analysis in ultrasonic tissue characterization," *J. Acoust. Soc. America*, vol. 73, no. 4, pp. 1366–1373, 1983.

[2] J. Mamou and M. L. Oelze, *Quantitative ultrasound in soft tissues*. Springer, 2013.

[3] E. J. Feleppa, J. Mamou, C. R. Porter, and J. Machi, "Quantitative ultrasound in cancer imaging," in *Seminars in oncology*, vol. 38, no. 1. Elsevier, 2011, pp. 136–150.

[4] M. L. Oelze, J. P. Kemmerer, G. Ghoshal, and R. M. Vlad, "Therapy monitoring and assessment using quantitative ultrasound," in *Quantitative Ultrasound in Soft Tissues*. Springer, 2013, pp. 193–216.

[5] M. F. Insana, T. J. Hall, J. G. Wood, and Z. Y. Yan, "Renal ultrasound using parametric imaging techniques to detect changes in microstructure and function," *Investigative radiology*, vol. 28, no. 8, pp. 720–725, 1993.

[6] N. Maklad, J. Ophir, and V. Balsara, "Attenuation of ultrasound in normal liver and diffuse liver disease in vivo," *Ultrason. Imaging*, vol. 6, no. 2, pp. 117–125, 1984.

[7] R. Kuc and M. Schwartz, "Estimating the acoustic attenuation coefficient slope for liver from reflected ultrasound signals," *IEEE Trans. Sonics Ultrason.*, vol. 26, no. 5, pp. 353–361, 1979.

[8] R. Kuc, "Clinical application of an ultrasound attenuation coefficient estimation technique for liver pathology characterization," *IEEE Trans. Biomed Eng*, no. 6, pp. 312–319, 1980.

[9] C. Langton, S. Palmer, and R. Porter, "The measurement of broadband ultrasonic attenuation in cancellous bone," *Eng Med*, vol. 13, no. 2, pp. 89–91, 1984.

[10] Y. Fujii, N. Taniguchi, K. Itoh, and K. Omoto, "Attenuation coefficient measurement in the thyroid," *J. ultrasound med*, vol. 22, no. 10, pp. 1067–1073, 2003.

[11] K. Nam, J. A. Zagzebski, and T. J. Hall, "Quantitative assessment of in vivo breast masses using ultrasound attenuation and backscatter," *Ultrason. Imaging*, vol. 35, no. 2, pp. 146–161, 2013.

[12] B. L. McFarlin, V. Kumar, T. A. Bigelow, D. G. Simpson, R. C. White-Traut, J. S. Abramowicz, and W. D. O'Brien Jr, "Beyond cervical length: A pilot study of ultrasonic attenuation for early detection of preterm birth risk," *Ultrasound Med. Biol.*, vol. 41, no. 11, pp. 3023–3029, 2015.

[13] F. Deeba, M. Ma, M. Pesteie, J. Terry, D. Pugash, J. A. Hutcheon, C. Mayer, S. Salcudean, and R. Rohling, "Attenuation coefficient estimation of normal placentas," *Ultrasound Med. Biol.*, vol. 45, no. 5, pp. 1081–1093, 2019.

[14] J. Ophir, N. Maklad, and R. Bigelow, "Ultrasonic attenuation measurements of in vivo human muscle," *Ultrason. Imaging*, vol. 4, no. 3, pp. 290–295, 1982.
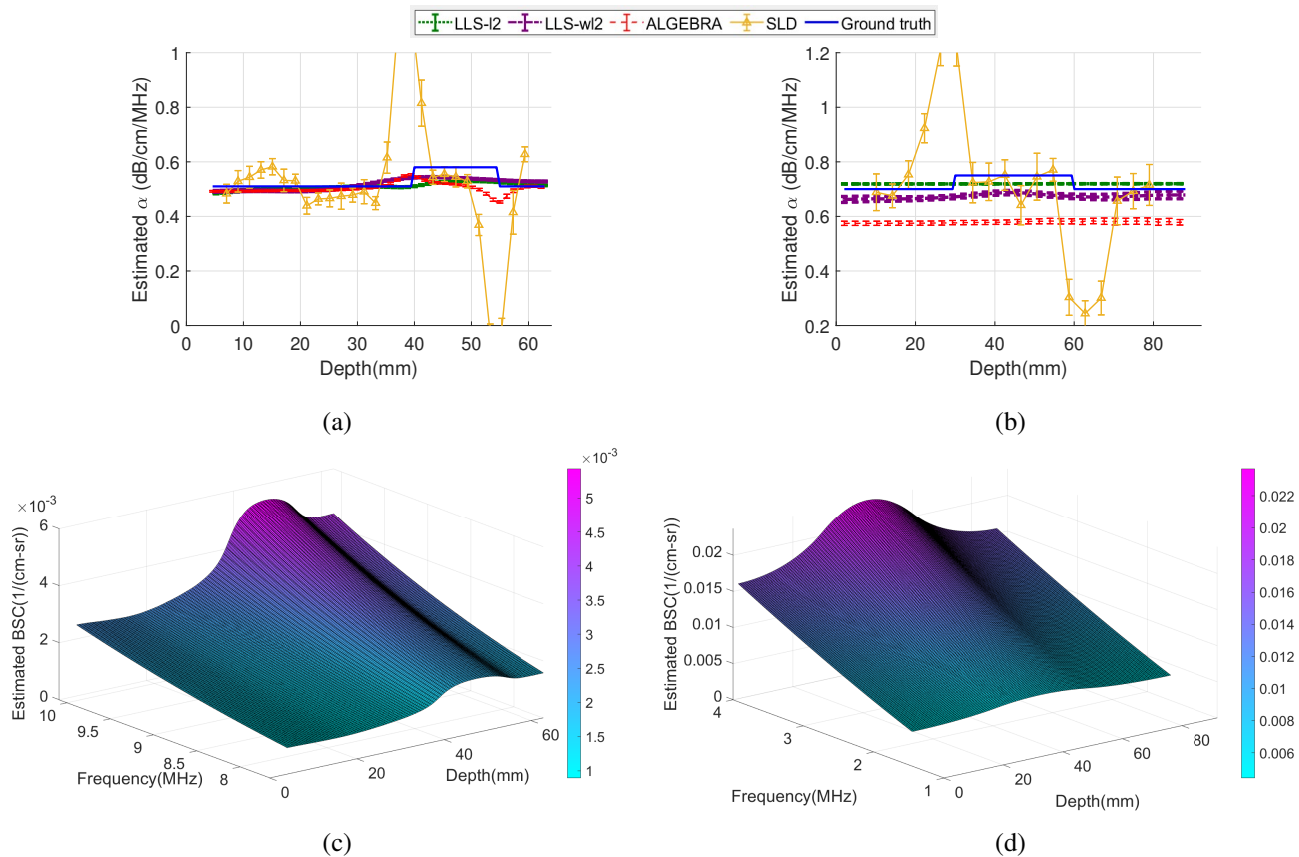
Fig. 11. Results of attenuation (α) and backscatter coefficient (BSC) estimation in a medium with varying BSC and nearly uniform α on the phantom data (subplots (a) and (c)) and simulated data (subplots (b) and (d)) in the left and right columns, respectively. Top row: α profile estimation results are shown. In each case, the mean estimated values are plotted, with the error bars denoting the standard deviation of the estimated values for 10 RF data frame/experimental trials. Bottom row: BSC profile estimation by LLS-l2 is plotted as a function of frequency and depth.

[15] R. Kuc, M. Schwartz, and L. Micsky, "Parametric estimation of the acoustic attenuation coefficient slope for soft tissue," in *1976 Ultrasonics Symposium.* IEEE, 1976, pp. 44–47.

[16] M. Insana, J. Zagzebski, and E. Madsen, "Improvements in the spectral difference method for measuring ultrasonic attenuation," *Ultrason. imaging*, vol. 5, no. 4, pp. 331–345, 1983.

[17] L. X. Yao, J. A. Zagzebski, and E. L. Madsen, "Backscatter coefficient measurements using a reference phantom to extract depth-dependent instrumentation factors," *Ultrason. Imaging*, vol. 12, no. 1, pp. 58–70, 1990.

[18] H. Kim and T. Varghese, "Hybrid spectral domain method for attenuation slope estimation," *Ultrasound Med. Biol.*, vol. 34, no. 11, pp. 1808–1819, 2008.

[19] K. Nam, J. A. Zagzebski, and T. J. Hall, "Simultaneous backscatter and attenuation estimation using a least squares method with constraints," *Ultrasound Med. Biol.*, vol. 37, no. 12, pp. 2096–2104, 2011.

[20] A. L. Coila and R. Lavarello, "Regularized spectral log difference technique for ultrasonic attenuation imaging," *IEEE Trans. Ultrason., Ferroelectr., Freq. Control*, vol. 65, no. 3, pp. 378–389, 2017.

[21] S. Boyd, N. Parikh, and E. Chu, *Distributed optimization and statistical learning via the alternating direction method of multipliers.* Now Publishers Inc, 2011.

[22] H. Chahuara, A. Basarab, and R. Lavarello, "Regularized framework for simultaneous estimation of ultrasonic attenuation and backscatter coefficients," in *2020 IEEE International Ultrasonics Symposium (IUS).* IEEE, 2020, pp. 1–4.

[23] F. Deeba, R. Hu, J. Terry, D. Pugash, J. A. Hutcheon, C. Mayer, S. Salcudean, and R. Rohling, "A spatially weighted regularization method for attenuation coefficient estimation," in *2019 IEEE International Ultrasonics Symposium (IUS).* IEEE, 2019, pp. 2023–2026.

[24] Z. Vajihi, I. M. Rosado-Mendez, T. J. Hall, and H. Rivaz, "Low variance estimation of backscatter quantitative ultrasound parameters using dynamic programming," *IEEE Trans. Ultrason., Ferroelectr., Freq. Control*, vol. 65, no. 11, pp. 2042–2053, 2018.

[25] Z. Vajihi, I. Rosado-Mendez, T. J. Hall, and H. Rivaz, "L1 and l2 norm depth-regularized estimation of the acoustic attenuation and backscatter coefficients using dynamic programming," in *2019 IEEE 16th International Symposium on Biomedical Imaging (ISBI 2019).* IEEE, 2019, pp. 1749–1752.

[26] A. Muraleedharan, A. Bertrand, and J. D'hooge, "A linear least squares estimation of spatially variant attenuation from ultrasound backscatter signals," in *Proceedings of Meetings on Acoustics.* Acoustical Society of America, 2019.

[27] J. Birdi, A. Muraleedharan, J. D'hooge, and A. Bertrand, "Fast linear least-squares method for ultrasound attenuation and backscatter estimation," *Ultrasonics*, p. 106503, 2021.

[28] N. Jafarpisheh, T. J. Hall, H. Rivaz, and I. M. Rosado-Mendez, "Analytic global regularized backscatter quantitative ultrasound," *IEEE Trans. Ultrason., Ferroelectr., Freq. Control*, vol. 68, no. 5, pp. 1605–1617, 2020.

[29] S. Nooijens, H. Hewener, M. Ingram, J. Birdi, A. Muraleedharan, S. Tretbar, A. Bertrand, M. Fournelle, and J. D'hooge, "Real-time attenuation estimation on an experimental ultrasound system," in *2021 IEEE International Ultrasonics Symposium (IUS).* IEEE, 2021.

[30] Y. Labyed and T. A. Bigelow, "A theoretical comparison of attenuation measurement techniques from backscattered ultrasound echoes," *J. Acoust. Soc. America*, vol. 129, no. 4, pp. 2316–2324, 2011.

[31] K. Nam, I. M. Rosado-Mendez, L. A. Wirtzfeld, A. D. Pawlicki, V. Kumar, E. L. Madsen, G. Ghoshal, R. J. Lavarello, M. L. Oelze, T. A. Bigelow *et al.*, "Ultrasonic attenuation and backscatter coefficient estimates of rodent-tumor-mimicking structures: comparison of results among clinical scanners," *Ultrason. imaging*, vol. 33, no. 4, pp. 233–250, 2011.

[32] S. W. Flax, N. J. Pelc, G. H. Glover, F. D. Gutmann, and M. McLachlan, "Spectral characterization and attenuation measurements in ultrasound," *Ultrason. Imaging*, vol. 5, no. 2, pp. 95–116, 1983.

[33] S. Gilbert, *Introduction to linear algebra.* Wellesley-Cambridge Press Wellesley, MA, 1993, vol. 3.

[34] J. A. Scales and A. Gersztenkorn, "Robust methods in inverse theory," *Inverse problems*, vol. 4, no. 4, p. 1071, 1988.

[35] J. Fox and S. Weisberg, "Robust regression," *An R and S-Plus companion to applied regression*, vol. 91, 2002.

[36] E. J. Candes, M. B. Wakin, and S. P. Boyd, "Enhancing sparsity by reweighted ℓ_1 minimization," *J. Fourier Anal Appl*, vol. 14, no. 5, pp. 877–905, 2008.

[37] H. J. Nussbaumer, "The fast fourier transform," in *Fast Fourier Transform and Convolution Algorithms*. Springer, 1981, pp. 80–111.

[38] M. C. Ziskin, "Fundamental physics of ultrasound and its propagation in tissue." *Radiographics*, vol. 13, no. 3, pp. 705–709, 1993.

[39] V. R. Amin, "Ultrasonic attenuation estimation for tissue characterization," Master's thesis, Iowa State University, USA, 1989.

[40] K. Nam, I. M. Rosado-Mendez, L. A. Wirtzfeld, G. Ghoshal, A. D. Pawlicki, E. L. Madsen, R. J. Lavarello, M. L. Oelze, J. A. Zagzebski, W. D. O'Brien Jr *et al.*, "Comparison of ultrasound attenuation and backscatter estimates in layered tissue-mimicking phantoms among three clinical scanners," *Ultrason. Imaging*, vol. 34, no. 4, pp. 209–221, 2012.

[41] H. G. Nasief, I. M. Rosado-Mendez, J. A. Zagzebski, and T. J. Hall, "Acoustic properties of breast fat," *Journal of Ultrasound in Medicine*, vol. 34, no. 11, pp. 2007–2016, 2015.

[42] N. Jafarpisheh, I. M. Rosado-Mendez, T. J. Hall, and H. Rivaz, "Regularized estimation of effective scatterer size and acoustic concentration quantitative ultrasound parameters using dynamic programming," in *2020 42nd Annual International Conference of the IEEE Engineering in Medicine & Biology Society (EMBC)*. IEEE, 2020, pp. 13–16.